Contrib Mineral Petrol (2014) 167:979
DOI 10.1007/s00410-014-0979-5

ORIGINAL PAPER

The high-pressure stability of chlorite and other hydrates in subduction mélanges: experiments in the system Cr_2O_3–MgO–Al_2O_3–SiO_2–H_2O

Patrizia Fumagalli · Stefano Poli · Johannes Fischer · Marco Merlini · Mauro Gemmi

Received: 17 July 2013 / Accepted: 30 January 2014 / Published online: 15 February 2014

Abstract The solubility of chromium in chlorite as a function of pressure, temperature, and bulk composition was investigated in the system Cr_2O_3–MgO–Al_2O_3–SiO_2–H_2O, and its effect on phase relations evaluated. Three different compositions with $X_{Cr} = Cr/(Cr + Al) = 0.075$, 0.25, and 0.5 respectively, were investigated at 1.5–6.5 GPa, 650–900 °C. Cr-chlorite only occurs in the bulk composition with $X_{Cr} = 0.075$; otherwise, spinel and garnet are the major aluminous phases. In the experiments, Cr-chlorite coexists with enstatite up to 3.5 GPa, 800–850 °C, and with forsterite, pyrope, and spinel at higher pressure. At $P > 5$ GPa other hydrates occur: a Cr-bearing phase-HAPY ($Mg_{2.2}Al_{1.5}Cr_{0.1}Si_{1.1}O_6(OH)_2$) is stable in assemblage with pyrope, forsterite, and spinel; Mg-sursassite coexists at 6.0 GPa, 650 °C with forsterite and spinel and a new Cr-bearing phase, named 11.5 Å phase (Mg:Al:Si = 6.3:1.2:2.4) after the first diffraction peak observed in high-resolution X-ray diffraction pattern. Cr affects the stability of chlorite by shifting its breakdown reactions toward higher temperature, but Cr solubility at high pressure is reduced compared with the solubility observed in low-pressure occurrences in hydrothermal environments. Chromium partitions generally according to $X_{Cr}^{spinel} \gg X_{Cr}^{opx} > X_{Cr}^{chlorite} \geq X_{Cr}^{HAPY} > X_{Cr}^{garnet}$. At 5 GPa, 750 °C (bulk with $X_{Cr} = 0.075$) equilibrium values are $X_{Cr}^{spinel} = 0.27$, $X_{Cr}^{chlorite} = 0.08$, $X_{Cr}^{garnet} = 0.05$; at 5.4 GPa, 720 °C $X_{Cr}^{spinel} = 0.33$, $X_{Cr}^{HAPY} = 0.06$, and $X_{Cr}^{garnet} = 0.04$; and at 3.5 GPa, 850 °C $X_{Cr}^{opx} = 0.12$ and $X_{Cr}^{chlorite} = 0.07$. Results on Cr–Al partitioning between spinel and garnet suggest that at low temperature the spinel- to garnet-peridotite transition has a negative slope of 0.5 GPa/100 °C. The formation of phase-HAPY, in assemblage with garnet and spinel, at pressures above chlorite breakdown, provides a viable mechanism to promote H_2O transport in metasomatized ultramafic mélanges of subduction channels.

Keywords Subduction mélanges · Earth mantle · Cr-chlorite · Spinel- to garnet-peridotite transition · Phase-HAPY

Introduction

Although chromium is a minor constituent of the Earth mantle, it is incorporated in almost all major mantle phases, i.e., spinels, garnets, and pyroxenes, and it is expected to substantially modify phase equilibria in both mafic and ultramafic rocks. Natural spinel or garnet lherzolites contain 2,600 ppm chromium on average (O'Neill and Palme 1998); pyroxenites can host a variable amount of chromium, from up to 3,400 ppm on average of chromium in the pyroxenites of Beni Boussera (Pearson et al. 1993; Kumar et al. 1996) to 2,400 ppm in Balmuccia pyroxenites (Mukasa and Shervais 1999; Sinigoi et al. 1983; Voshage et al. 1988). In the mantle, at moderate pressures,

Communicated by T. L. Grove.

Electronic supplementary material The online version of this article (doi:10.1007/s00410-014-0979-5) contains supplementary material, which is available to authorized users.

P. Fumagalli (✉) · S. Poli · J. Fischer · M. Merlini
Dipartimento di Scienze Della Terra "Ardito Desio", Università degli Studi di Milano, Via Botticelli 23, 20133 Milan, Italy
e-mail: patrizia.fumagalli@unimi.it

M. Gemmi
Center for Nanotechnology Innovation@NEST, Istituto Italiano di Tecnologia, Pisa, Italy

chromium is mainly hosted in spinel, containing 10–32 wt% of Cr_2O_3, followed by 3–5 wt% in garnet, 0.2–0.6 wt% in orthopyroxene, and up to 0.02 wt% in olivine (Hervig and Smith 1982). At higher pressure, garnet becomes one of the major hosts of chromium, as testified by the occurrence of garnet with up to 22 wt% Cr_2O_3 (up to 65 % mole fraction of knorringite—$Mg_3Cr_2Si_3O_{12}$) in deep mantle xenoliths (Stachel and Harris 2008) and in inclusions in diamonds (Sobolev et al. 2004; Meyer 1975).

Chromium has also a strong influence on the spinel to garnet transition, usually taken as reference for the pressure evolution of mantle rocks (Klemme 2004).

The simple system $MgO–Al_2O_3–SiO_2–H_2O$ (MASH) has been widely used not only to model hydrated mantle rocks (Ulmer and Trommsdorff 1999), but also to investigate a variable range of lithologies at the slab–mantle interface, where mass transfer in mélange zones generates hybrid rocks. Particular emphasis has been given to the role of chlorite-rich schists (Marschall and Schumacher 2012) and therefore to the Al-rich compositional space in the system MASH. Although chlorite is the most important hydrate mineral in this system, a new Hydrous Al-bearing PYroxene-like phase (phase-HAPY—$Mg_{2.1}Al_{0.9}(OH)_2Al_{0.9}Si_{1.1}O_6$, Gemmi et al. 2011) has been recently recognized at pressures beyond clinochlore stability and found to be relevant to the transport of water to depth exceeding 150 km in locally Al-enriched hybrid rocks in subduction environments (Bebout 2007; Spandler et al. 2008). Nonetheless, this Al-rich and H_2O-rich part of the system remains only poorly investigated.

Phase equilibria in the system MASH are expected to be strongly modified, due to the uneven fractionation of Cr^{3+} among major mantle phases (Chatterjee and Terhart 1985). Experiments so far investigated the effect of chromium in dry systems, carefully focusing on high-temperature partitioning between spinel and garnet (Klemme and O'Neill 2000) or dealing with the effect of chromium on Al solubility in orthopyroxene (Klemme 2004). The role of hydrates, additional candidates for hosting Cr into their structure in "metasomatized" ultramafics, has not been evaluated yet.

The stability of chlorite in the model system MASH is critical in the modelling of the hydration/dehydration sequence in "altered" ultramafic rocks, which include both serpentinized peridotites and metasomatized either on the ocean floor or along outer-rise normal faults at subduction trenches (Peacock 2001). Other hybrid rocks occur in various subduction settings, both at the top of the slab (Spandler et al. 2008; Bebout 2007) and in the wedge (Smith 2010). In hydrated ultramafic systems, chlorite (containing 13 wt% of H_2O) is a good candidate for transferring water beyond the stability field of antigorite, being stable up to 4–6 GPa, 700–800 °C. Chromium solubility in chlorite may further extend its stability and likely influence phase relations. Chromian chlorites of hydrothermal origin (Erzincan Chlorite, Turkey) have been known to contain up to 9.3 wt% Cr_2O_3 (Brown and Bailey 1963; Welch and Crichton 2005). High-pressure mantle chlorite, found in natural peridotites, hosts up to 2.0 wt% Cr_2O_3 (Ravna 2006); intermediate contents of Cr_2O_3 (up to 5–6 wt%) have been reported for chromian chlorite found in veins in association with chromite deposits and ultramafics (e.g., Niuggihalli Schist Belt, India—5.18 wt% Cr_2O_3). Grove et al. (2006) and Till et al. (2012) synthesized chlorites containing up to 1.47 wt% Cr_2O_3 at 3.6 GPa, 800 °C, in a bulk composition representing a model primitive mantle peridotite.

Phase equilibria studies in peridotites modelled in the Cr-free system $Na_2O–CaO–FeO–MASH$ (Fumagalli and Poli 2005) reveal that, as a results of preferential partitioning of Fe into garnet, chlorite breaks down to garnet + olivine + pyroxenes at approx. 780 °C and at 3 GPa. In experiments performed in fluid-saturated Cr-bearing peridotite systems, Grove et al. (2006) reported the assemblage olivine + orthopyroxene + clinopyroxene + garnet + chlorite + ilmenite + "glass" at 840 °C and 2.8 GPa.

The goals of this work are (1) to evaluate the influence of Cr on the high-temperature stability of chlorite at high pressure; (2) to estimate the Cr partitioning between chlorite and coexisting anhydrous phases, and, thereby, offer further constraints on the pyrope + forsterite = spinel + enstatite divariant loop; and (3) to explore phases that form as a consequence of chlorite breakdown at high pressure.

Phase equilibria in the MASH system: previous experimental constraints

Phase relations in the system MASH relevant for hydrated mantle bulk compositions have been reviewed by Ulmer and Trommsdorff (1999) based on available experimental data. Figure 1 shows phase equilibria in the system MASH for pressures higher than 2 GPa. Phases involved in the four invariant points are forsterite, enstatite, spinel, pyrope, diaspore/corundum, and the two hydrous silicates chlorite and Mg-sursassite. Invariant point I involves spinel, enstatite, forsterite, pyrope, and chlorite, with four main reactions. The first represents the extensively studied spinel to garnet transition (the high-temperature assemblages are on the right side of the equations)

$$\text{pyrope} + \text{forsterite} = \text{spinel} + \text{enstatite} \quad (1)$$

The other three control the thermal stability of chlorite and are the terminal reaction in the spinel stability field

$$\text{chlorite} = \text{spinel} + \text{enstatite} + \text{forsterite} + H_2O, \quad (2)$$

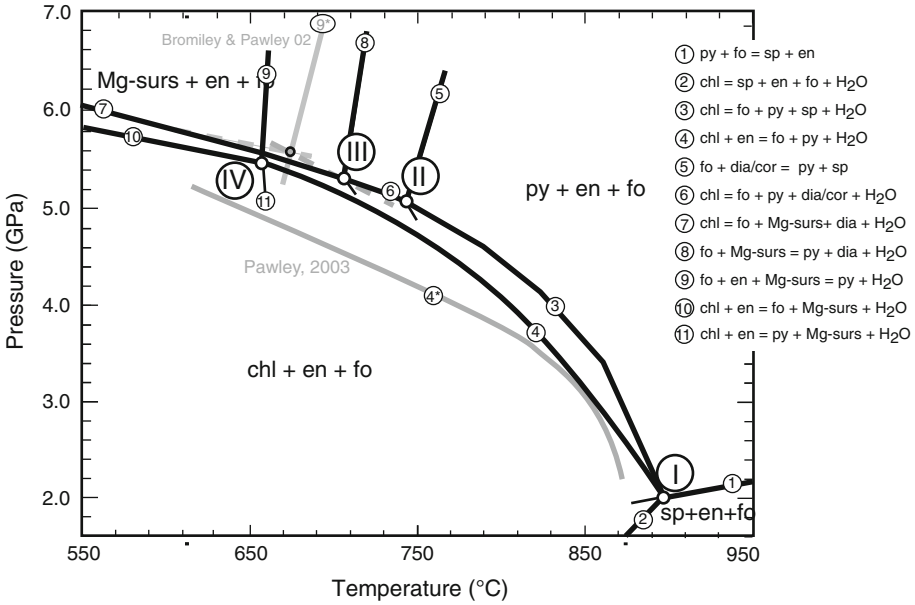

Fig. 1 Phase relations in the $MgO–Al_2O_3–SiO_2–H_2O$ system as reported by Ulmer and Trommsdorff (1999), experimentally constrained by Fockenberg (1995). *chl* clinochlore, *en* enstatite, *fo* forsterite, *sp* spinel, *py* pyrope, *Mg-surs* Mg-sursassite, *dia* diaspore, *cor* corundum. *Star* on numbers marks the location of reactions after experimental results of Pawley (2003) and Bromiley and Pawley (2002)

occurring within the stability field of spinel, extensively investigated and constrained by Staudigel and Schreyer (1977), Jenkins (1981), and Jenkins and Chernosky (1986); the terminal reaction within the garnet stability field

$$2\,\text{chlorite} = 3\,\text{forsterite} + 1\,\text{pyrope} + 1\,\text{spinel} + 8\,H_2O \quad (3)$$

investigated by Staudigel and Schreyer (1977) and Fockenberg (1995); and the breakdown reaction for chlorite + enstatite assemblages

$$1\,\text{chlorite} + 1\,\text{enstatite} = 2\,\text{forsterite} + 1\,\text{pyrope} + 4\,H_2O. \quad (4)$$

The thermal stability of chlorite on its own composition has been suggested to be very similar to the thermal stability of chlorite + enstatite (Ulmer and Trommsdorff 1999). However, subsequent reversal experiments (Pawley 2003) shifted the location of reaction (4) toward lower temperatures, increasing the thermal difference between the two-phase boundaries.

Reaction (3) intersects the invariant point II that involves chlorite, enstatite, pyrope, diaspore/corundum, and forsterite. The location of invariant point II is not well constrained, as it is based on just a few experiments on the stability of the forsterite + diaspore assemblage (Fockenberg 1995) controlled by

$$\text{forsterite} + \text{corundum} = \text{pyrope} + \text{spinel} \quad (5)$$

As a result of Schreinemakers' analysis, the reaction

$$\text{chlorite} = \text{forsterite} + \text{pyrope} + \text{diaspore/corundum} + H_2O \quad (6)$$

has been located between invariant point II and invariant point III.

Invariant point III implies the stability of Mg-sursassite, previously known as MgMgAl-pumpellyite, Schreyer et al. (1986), Artioli et al. (1999), Fockenberg (1995), and subsequently re-named Mg-sursassite, Gottschalk et al. (2000). This stability is mutually controlled by reactions that stabilize the pyrope + H_2O join. Mg-sursassite would form as a product of the chlorite breakdown reaction

$$\text{chlorite} = \text{forsterite} + \text{Mg-sursassite} + \text{diaspore} + H_2O, \quad (7)$$

constrained by experiments of Fockenberg (1995) who found the assemblage forsterite, diaspore, and Mg-sursassite starting from 5.4 GPa, 700 °C, and thermally constrained by the reaction

$$\text{forsterite} + \text{Mg-sursassite} = \text{pyrope} + \text{diaspore} + H_2O. \quad (8)$$

At the lowest temperature investigated, the invariant point IV involves chlorite, Mg-sursassite, forsterite, enstatite, and pyrope, and controls the location of the reaction

$$\text{forsterite} + \text{enstatite} + \text{Mg-sursassite} = \text{pyrope} + H_2O, \quad (9)$$

bracketed by Bromiley and Pawley (2002) and shown as reaction 9* in Fig. 1, and of the reaction

$$\text{chlorite} + \text{enstatite} = \text{forsterite} + \text{Mg - sursassite} + H_2O. \quad (10)$$

At pressures higher than 7 GPa, reaction (9) has been bracketed by Fockenberg (2008) who found pyrope plus H_2O at temperatures as low as 630 °C, at 6.4 GPa, a

temperature considerably lower than that determined by Bromiley and Pawley (2002).

This study is mainly aimed to evaluate the effect of Cr on the thermal stability of Cr-chlorite related to reaction (4), to draw further constraints on the reactions controlling the occurrence of other hydrous silicates beyond the chlorite stability field, and to evaluate the Cr partitioning at temperatures characteristic of subduction environments.

Experimental procedures

Starting materials

Experiments were performed in the system Cr_2O_3–MgO–Al_2O_3–SiO_2–H_2O. Starting from a clinochlore composition $Mg_5Al_2Si_3O_{10}(OH)_8$, three different bulk compositions were prepared: bulk A with Cr/(Cr + Al) = 0.075; bulk B with Cr/(Cr + Al) = 0.25, and bulk C with Cr/(Cr + Al) = 0.5 (Table 1; Fig. 2). Three additional bulk compositions (AT, JK and JO) were prepared to investigate poorly explored parts of the MASH system.

Bulk composition JK is close to the average Cr-bearing phase-HAPY, first detected at 5.2 GPa, 700 °C in bulk A (Gemmi et al. 2011); bulk AT lies on the join pyrope–spinel; bulk JO lies on the join pyrope–phase A, and simulates the composition of an additional phase, characterized by its first diffraction peak at 11.5 Å, revealed in bulk A at 6.0 GPa, 650 °C. To promote equilibrium at subsolidus temperatures, gels were prepared using tetraethylorthosilicate as the silica source, and pure Cr-, Mg-, and Al-nitric solutions, following the method of Hamilton and

Table 1 Compositions of starting materials in wt% of oxides and atomic proportions

	Bulk A	Bulk B	Bulk C	Chl	Bulk AT	Bulk JK	Bulk JO
SiO_2	36.99	36.31	35.44	34.10 (0.17)	38.51	27.32	31.25
Al_2O_3	19.39	15.41	10.01	12.20 (0.14)	31.19	36.87	12.50
Cr_2O_3	2.34	7.66	14.91	0.06 (0.02)	–	–	–
FeO	–	–	–	4.89 (0.07)	–	–	–
MgO	41.28	40.62	39.64	33.80 (0.12)	30.29	35.81	56.25
Total	100.00	100.00	100.00	84.85	100.00	100.00	100.00
Si	6.000	6.000	6.000	6.610 (0.017)	6.396	4.400	4.814
Al	3.700	3.000	2.000	2.790 (0.030)	6.105	7.000	2.270
Cr	0.300	1.000	2.000	0.009 (0.004)	–	–	–
Fe	–	–	–	0.793 (0.013)			
Mg	10.000	10.000	10.000	9.780 (0.016)	7.499	8.599	12.916
Cr/(Cr + Al)	0.075	0.250	0.500	–	–	–	–

Chl: averages of 10 analyses and standard deviations (in parentheses) of natural monoclinic clinochlore from Val Malenco (Italy) used as seeds; fitted cell parameters are $a = 5.3398(4)$ Å; $b = 9.2571(7)$ Å; $c = 14.513(1)$ Å; $\beta = 97.06(2)$

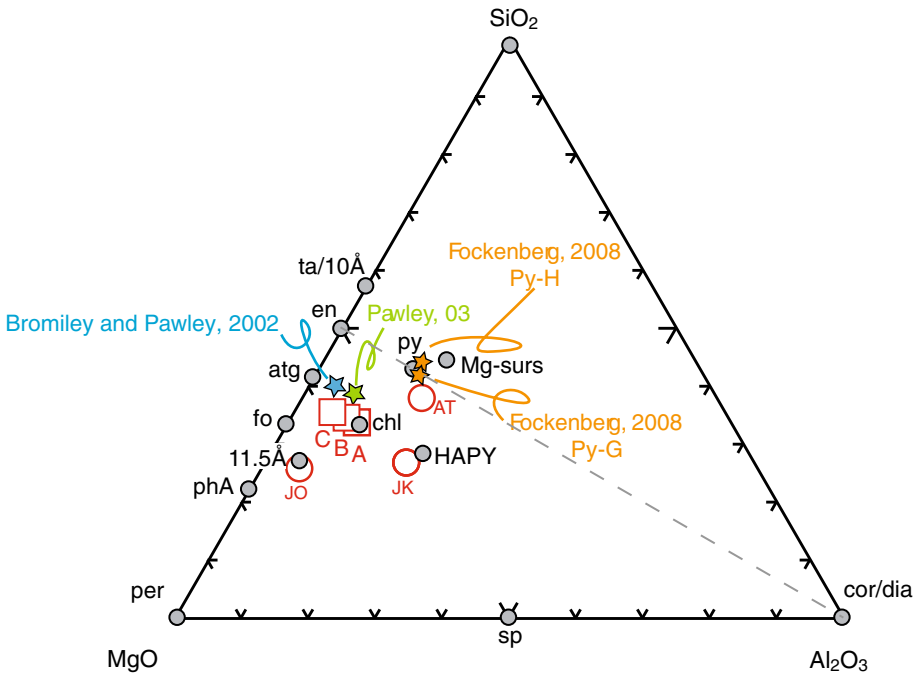

Fig. 2 Compositions (in mol%) of the starting materials investigated (see also Table 1) plotted in the system MgO–Al_2O_3–SiO_2 with H_2O in excess (MASH), as compared to bulk compositions investigated in previous studies. Most relevant phases in the MgO–SiO_2–H_2O system are also shown; *chl* clinochlore, *en* enstatite, *fo* forsterite, *sp* spinel, *ta* talc, *10Å* 10Å phase, *atg* antigorite, *phA* phase A, *py* pyrope, *Mg-surs* Mg-sursassite, *per* periclase, *dia* diaspore, *cor* corundum, *11.5* 11.5 Å phase, *HAPY* phase-HAPY—High-Aluminum PYroxene (Gemmi et al. 2011)

Henderson (1968). In order to promote crystal growth rather than nucleation, gels were seeded with 5 wt% of natural monoclinic clinochlore (Val Malenco, Italy; see Table 1). The seeds contain about 5 wt% FeO introducing up to 0.25 wt% of FeO in the bulk; this causes a slight deviation from the nominally Fe-free model chemical system Cr–MASH. Nonetheless, FeO is a minor component, and its influence is assumed to be negligible.

Experimental techniques

Experiments were performed at the Dipartimento di Scienze della Terra (University of Milan—UMI, Italy) at pressures ranging from 1.5 to 6.5 GPa and temperatures from 650 to 900 °C (Table 2). Pressures lower than 3.4 GPa were investigated in both single-stage (up to 1.8 GPa) and end-loaded (up to 3.4 GPa) piston cylinders using full-salt and MgO-salt assemblies, respectively. Temperature was measured by K-type and S-type thermocouples and was considered to be accurate to ±5 °C. A Walker type multi-anvil apparatus was used for higher pressures using tungsten carbide cubes of 32-mm-edge length and 17 mm truncation, and pressure cells made of prefabricated MgO–Cr_2O_3 octahedra with a 25-mm-edge length. Multi-anvil pressure calibration was performed both at room temperature, using the phase transitions Bi I–II, Bi III–V (respectively, at 2.55 and 7.7 GPa), and, at 1,000 °C, using the coesite–stishovite and the $CaGeO_3$ garnet–perovskite transitions at 8.7 GPa (Zhang et al. 1996) and 6.1 GPa (Suzaki et al. 1985). Pressure uncertainties were assumed to be ±3 %. Further details are given by Fumagalli and Poli (1999). Temperature was measured by S-type thermocouples and was considered to be accurate to ±20 °C without taking into account any effect of pressure on the electromotive force. Seeded gels were loaded into gold capsules of 3 mm of outer diameter. All experiments were performed at fluid-saturated conditions. About 20 wt% of distilled H_2O was introduced by a microsyringe. The capsules were welded and after quenching tested for the presence of a free fluid phase. Runs lasted up to 289 h.

Table 2 Run conditions and run products

RUN	BULK	*P* (GPa)	*T* (°C)	Run time (h)	Run products
JF-2 (SS-PC)	A	2.0	800	172	Cr-chlorite (91), orthopyroxene (9)
JF-7 (EL-PC)	A	3.5	800	176	Cr-chlorite (99.5), orthopyroxene (0.5)
A 5 (EL-PC)	A	3.5	850	139	Cr-chlorite (91), orthopyroxene (9)
JF-9 (EL-PC)	A	3.5	900	67	Garnet, forsterite, spinel
A14 (MA)	A	4.2	840	124	Garnet, forsterite, spinel
A13 (MA)	A	4.8	780	105	Garnet, forsterite, spinel
A 6 (MA)	A	5.0	750	124	Cr-chlorite, garnet, forsterite, spinel
A 9 (MA)	A	5.0	800	150	Garnet, forsterite, spinel
A 10 (MA)	A	5.4	700	73	Garnet, forsterite, spinel, phase-HAPY, diaspore
A 12 (MA)	A	5.4	720	121	Garnet, forsterite, spinel, phase-HAPY
A 11 (MA)	A	5.5	670	144	Cr-chlorite, garnet, forsterite, spinel
A 7 (MA)	A	6.0	650	168	Sursassite, forsterite, spinel, 11.5 Å phase
A 8 (MA)	A	6.5	700	150	Garnet, forsterite, diaspore, guyanaite, 11.5 Å phase
JF-3 (SS-PC)	B	1.5	800	191.5	Orthopyroxene, forsterite, spinel
JF-5 (EL-PC)	B	3.5	750	216.5	Orthopyroxene(5), forsterite (81), spinel (14)
B 3 (EL-PC)	B	3.5	850	139	Orthopyroxene, forsterite, spinel
B 4 (MA)	B	5.0	750	124	Orthopyroxene, forsterite, spinel
B 5 (MA)	B	6.0	650	168	Orthopyroxene, forsterite, diaspore, guyanaite
JF-6 (EL-PC)	C	2.5	800	168	Orthopyroxene (7), forsterite (71), spinel (28)
JF-10 (EL-PC)	C	3.5	900	67	Orthopyroxene, forsterite, spinel
JO1 (MA)	JO*	6.5	700	218	Forsterite, 11.5 Å phase
JK1 (MA)	JK*	5.2	750	145	Phase-HAPY, pyrope, diaspore
JK2 (MA)	JK*	6.0	800	289	Pyrope (50), forsterite (12), spinel (38)
JK3 (MA)	JK*	6.5	700	218	Pyrope, forsterite, spinel
AT2 (MA)	AT*	5.4	720	148	Phase-HAPY, pyrope, diaspore

In parentheses are reported modal abundances of phases as retrieved by Rietveld refinements of X-ray powder diffraction. All but (*) are seeded bulks

Although the oxidation state within the capsule was not buffered directly, we assume that in all phases Cr was present in its most stable oxidation state, i.e., Cr^{3+}. Furthermore, the occurrence of significant Cr^{2+} is ruled out on the basis of the lack of Cr in olivine, as discussed by Klemme and O'Neill (2000).

Run products were identified by laboratory and synchrotron X-ray powder diffraction (XRPD), performed with a PanAlytical X'Pert instrument (Dipartimento di Scienze della Terra, UMI), and at ESRF—European Synchrotron Radiation Facility (Grenoble, France) with data collected at BM08, ID09A, and ID11 beamlines (BM08: wavelength 0.6878 Å, Fuji image plate detector; ID09: wavelength 0.4142 Å, mar555 flat panel detector; ID11: 0.4200 Å, Frelon area detector). The integration of the raw 2D data was performed with the Fit2D software (Hammersley et al. 1996), and Rietveld analysis was performed with the GSAS software (Larson and Von Dreele 1994). Mineral chemistry and BSE images were collected by electron microprobe using a JEOL JXA 8200 equipped with five WDS wavelength-dispersive spectrometers (Dipartimento di Scienze della Terra, UMI). Analyses were performed at 15 kV and 5 nA; natural and synthetic minerals were used as standards. All standards were calibrated within 0.5 % at one standard deviation. Raw data were corrected using a Phi–Rho–Z quantitative analysis program. Representative WDS analyses of mineral phases are reported in the Supplementary Material.

Approach to equilibrium

The attainment of equilibrium in complex systems and for continuous reactions is difficult to be demonstrated. Thus, we performed synthesis unreversed experiments. However, the approach to equilibrium was evaluated for each run through the following observations: (1) the growth of compositionally homogeneous, chemically unzoned minerals, likely favored by long run durations; (2) systematic and consistent variations in mineral chemistry and coherent element partitioning at different pressure and temperature conditions; and (3) constant bulk composition as gained by mass balance calculations.

Results: phase assemblages and textures

Experimental results are summarized in Table 2. Phase proportions, where available, are reported in parentheses and have been derived by XRPD Rietveld refinement. Phase relationships in the Cr–MASH system are reported in Fig. 3.

Cr-chlorite only occurs in bulk A ($X_{Cr} = Cr/(Cr + Al) = 0.075$, squares in Fig. 3). Chlorite coexists with orthopyroxene up to 3.5 GPa, 800–850 °C, and with pyrope, forsterite, and spinel at higher pressure (5.0 GPa, 670 °C; and 5.5 GPa, 750 °C). Chlorite-bearing assemblages at 2 GPa, 800 °C and 3.5 GPa, 850 °C appear as intergrowth of flakes of Cr-chlorite coexisting with elongated prismatic orthopyroxene (Fig. 4a). Large euhedral Cr-bearing pyrope and approx. 1–2 μm size isometric spinels and forsterite form at higher pressure (5.0 GPa, 750 °C and 5.5 GPa, 670 °C) in assemblage with Cr-chlorite (Fig. 4b). The 5-phase, Cr-chlorite–garnet–forsterite–spinel–fluid, divariant assemblage, unfeasible in the H_2O-saturated MASH system, is possible here because of the addition of a further component (i.e., Cr_2O_3).

The anhydrous assemblage garnet, forsterite, and spinel was found in bulk A at 4.8 GPa, 780 °C; 4.2 GPa, 840 °C; and 3.5 GPa, 900 °C, and in the MASH system in bulk JK at 6.5 GPa, 700 °C and 6 GPa, 800 °C. In bulk A, beyond the stability field of chlorite, isometric euhedral garnets are embedded in subhedral forsterite and in up to few μm size spinels, which are homogenously and randomly distributed.

At $P \geq 5.4$ GPa, a phase-HAPY with up to 3.21 wt% Cr_2O_3 was detected. It is homogenously distributed in assemblage with forsterite, pyrope, and spinel (Fig. 4c), suggesting the attainment of the Cr-clinochlore terminal reaction. X-ray powder diffraction of the multiphase assemblage containing phase-HAPY (run A10) is shown in Fig. 5a.

At 6.0 GPa, 650 °C (run A7) Mg-sursassite was found in assemblage with forsterite and spinel. At 6.5 GPa and 700 °C (run A8), the XRPD indicates the presence of pyrope, forsterite, CrO(OH) guyanaite, and diaspore. In addition, in runs A7 and A8, the diffraction patterns show also a few unknown diffraction peaks, which may indicate the presence of a new phase. Synchrotron high-resolution diffraction data clearly reveal several peaks that could not be matched with known phases in the Cr–MASH system, with the first unindexed peak at 11.5 Å (Fig. 5b). This is confirmed by SEM images, which show the presence of homogenously distributed large flaky minerals, which are several tens of micrometers of diameter often arranged in fan-like aggregates (Fig. 4d, e). Runs A8 and A10 represent univariant phase assemblages at fluid saturation. However, whether the phase assemblage indicates fluid undersaturation, or the occurrence of diaspore in these runs is the result of a metastable precipitation upon quenching is unclear. Both phase-HAPY and the 11.5 Å phase were successfully reproduced in synthesis experiments in the simple MASH system. Phase-HAPY was found in bulk JK at 5.2 GPa, 700 °C in assemblage with pyrope, diaspore, and an MgO-rich fluid as testified by precipitation of brucite during quenching (Stalder et al. 2001). The 11.5 Å phase was detected together with forsterite in bulk JO at 6.5 GPa and 700 °C. A detailed crystallographic

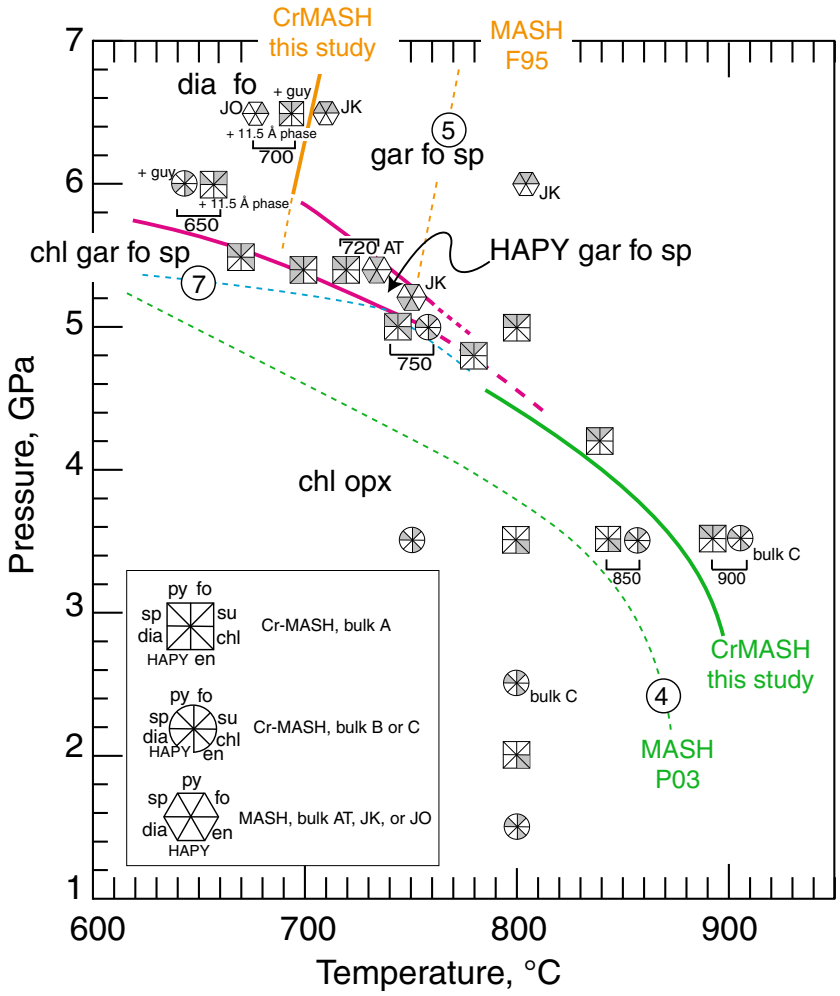

Fig. 3 Phase assemblages in Cr–MASH (bulk A, B, and C) and MASH (bulk JK, AT, and JO) systems. Reaction numbers as in Fig. 1; *F95* Fockenberg 1995, *P03* Pawley 2003; *opx* orthopyroxene, *gar* garnet, *guy* guyanaite; other abbreviations as in Fig. 2

investigation of phase-HAPY is reported by Gemmi et al. (2011), and further characterizations are in progress. At 6.5 GPa, 700 °C, and at 6.0 GPa, 800 °C, pyrope, forsterite, and spinel indicate the breakdown of phase-HAPY, in agreement with the reaction in the MASH system.

$$\text{phase-HAPY} = 7\,\text{forsterite} + 5\,\text{pyrope} + 13\,\text{spinel} + 20\,H_2O$$

Results on bulk AT further confirm the assemblage phase-HAPY, pyrope, and diaspore at 5.4 GPa, 720 °C.

No Cr-chlorite was found in bulk compositions B and C (circles); the anhydrous phase assemblage orthopyroxene, forsterite, spinel was found instead from 1.5 to 5.0 GPa and 750–850 °C. At higher pressure and lower temperatures (i.e., 6.0 GPa, 650 °C), guyanaite—CrO(OH)—was first detected by X-ray diffractometry and then analyzed at the microprobe. This phase coexisted with orthopyroxene, forsterite, and diaspore. In bulk compositions B and C, phase assemblages result in intergrowths of large elongated prismatic crystals of orthopyroxene and forsterite together with aggregates of smaller and randomly distributed spinels (Fig. 4f).

Chemical and structural properties of mineral phases synthesized in Cr–MASH system

Chlorite

Chlorite is compositionally close to clinochlore, $Mg_5Al_2Si_3O_{10}(OH)_8$; a slight deviation from the Cr–MASH system due to iron in chlorite crystal seeds accounts for the occurrence of up to 0.25 wt% of FeO in chlorite. In agreement with the coexistence with garnet, X_{Mg} in chlorite markedly increases with pressure, reaching values of <0.1 wt. FeO at 5.5 GPa, 670 °C.

The maximum Cr_2O_3 content in chlorite reaches 2.18 wt% corresponding to 0.343 a.p.f.u., at 5.5 GPa, 670 °C, *P–T* conditions close to the upper pressure stability (see Supplementary data). This Cr_2O_3 content is very close to the limit of 2.0 wt% reported by Lapham (1958) above which optical properties of chlorites would change (Lapham 1958; Phillips et al. 1980).

In order to gain crystal-chemical insights of chlorites, we performed structural analyses, with high-resolution

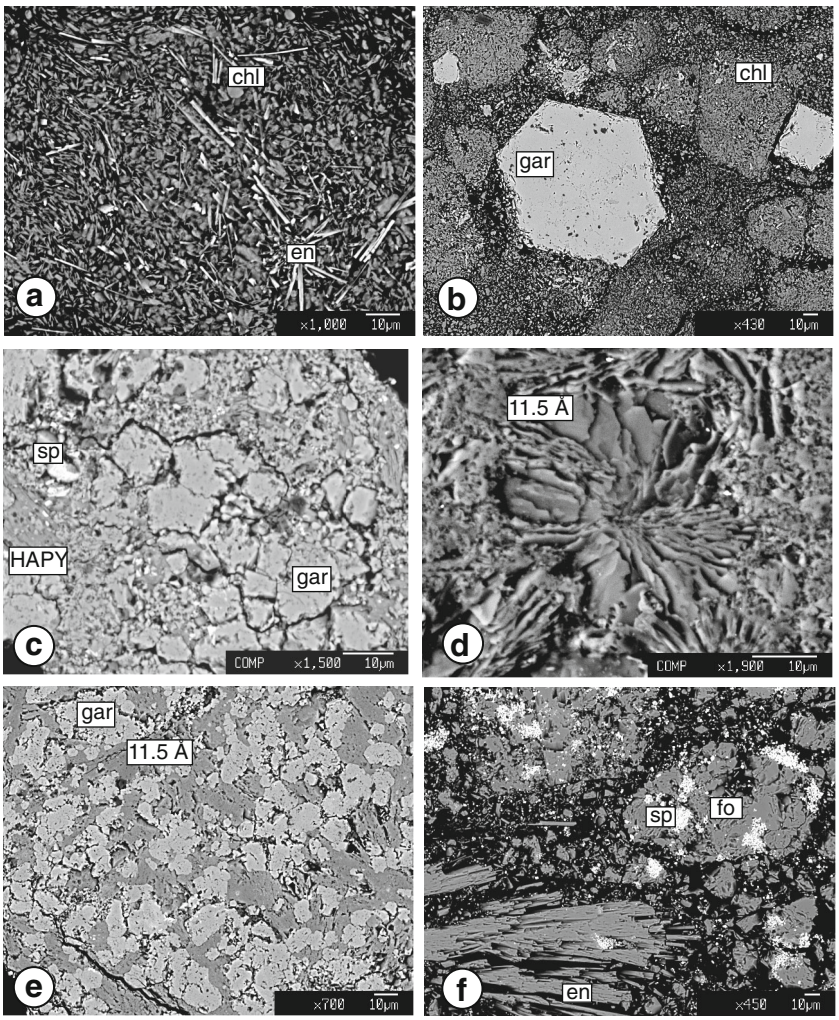

Fig. 4 Representative back-scattered electron images of run products; **a** chlorite and enstatite in bulk A at 3.5 GPa, 800 °C; **b** chlorite, pyrope, orthopyroxene, spinel in bulk A at 5.0 GPa, 750 °C; **c** phase-HAPY in assemblage with pyrope, forsterite, and spinel in bulk A at 5.2 GPa, 700 °C; bulk at, **d** the newly synthesized 11.5 Å phase in the MASH system, bulk JO, at 6.5 GPA, 700 °C; **e** 11.5 Å phase in the Cr–MASH system with garnet (+guyanite + diaspore) at 6.5 GPa, 700 °C; **f** enstatite, forsterite, spinel assemblage in bulk C at 2.5 GPa, 800 °C

synchrotron diffraction data (Fig. 6). The powder patterns of the chlorite-bearing samples are indexed by a triclinic unit cell ($a = 5.3237$ Å, $b = 9.2215$ Å, $c = 14.3785$ Å, $\alpha = 89.88°$, $\beta = 97.08°$, $\gamma = 89.99°$, $V = 700.5$ Å^3 at 2 GPa, 650 °C), and the diffraction intensities are well reproduced using the triclinic Cr-chlorite model (Brown and Bailey 1963; Phillips et al. 1980). The sharp hk0 and hkl peaks suggest a rather ordered stacking sequence. We noticed also several very weak diffraction peaks in the d-range 4.5–3.5 Å, which may be indexed if a 2-layer chlorite model ($c \approx 28.7$ Å) is adopted. However, the attempt to build a 2-layer structural model resulted in a poor matching of diffraction intensities. Moreover, if a triclinic symmetry is assumed, as indicated by the high-resolution synchrotron angular position, the 003 and 005 diffractions (present in the 10–5.5 Å d-range, non-overlapping with any other diffraction lines) would present a nonzero intensity, but this is not the case. A reasonable explanation would be the presence of a second chlorite phase with 2-layer periodicity. Refinements with two structural models, the triclinic Cr-bearing one, and a monoclinic 2-layer clinochlore, result in a phase fraction of 93 % of triclinic polymorph and 7 % of monoclinic one. This phase fraction indicates the possible presence of unreacted clinochlore seeds, even if a complex intergrowth of monoclinic and triclinic chlorite cannot be excluded. The predominance of one-layer triclinic chlorite, however, allowed a structural refinement, which confirmed the presence of Cr^{3+} in the octahedral interlayer. In fact, the unconstrained refinement of occupancies for the four octahedral sites converged with higher electron density in octahedral brucitic interlayer sites.

As a result, chlorite mineral chemistry is described in terms of two exchange vectors: $Mg_{-1}AlSi_{-1}Al$ (Tschermak component, active in the 2:1 layer) and $CrAl_{-1}$ (active in the brucite layer, preferentially in the M4 site). In Fig. 7a, the relation between Mg + Fe and Al + Cr a.p.f.u. is shown. The Tschermak component, represented by the arrow pointing toward the amesite end member

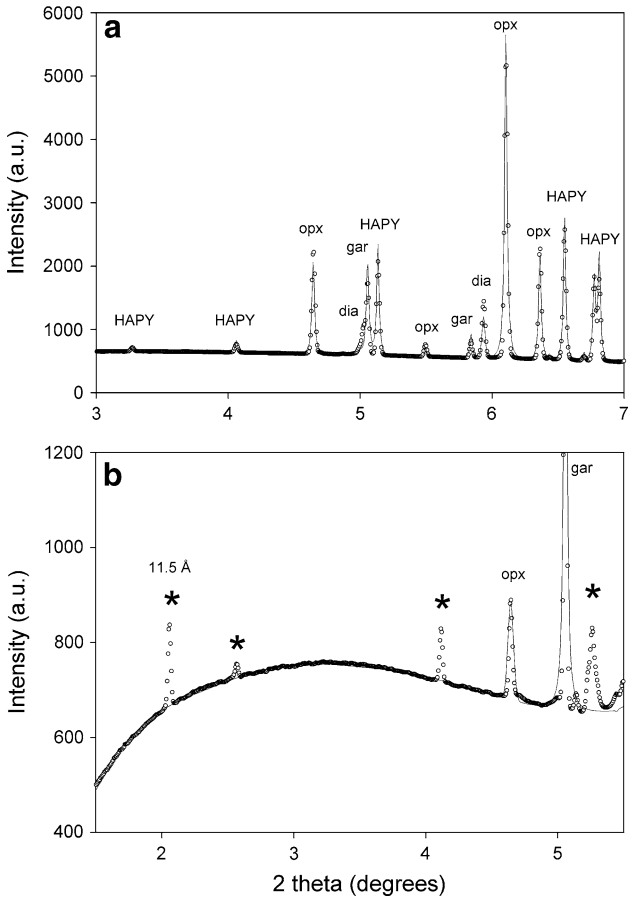

Fig. 5 **a** Low-angle portion of synchrotron X-ray powder pattern ($\lambda = 0.4142$ Å), and Rietveld refinement (*circles* observed intensity; *lines* calculated profile) of run at 5.4 and 700 °C (bulk A); *HAPY* phase-HAPY, *ol* olivine, *gar* garnet, *dia* diaspore; **b** Low-angle region of synchrotron X-ray powder pattern ($\lambda = 0.4142$ Å) and Rietveld refinement of the sample synthesized at 6.5 GPa and 700 °C (bulk A); labeled with stars are the diffraction peaks of the unknown 11.5 Å phase

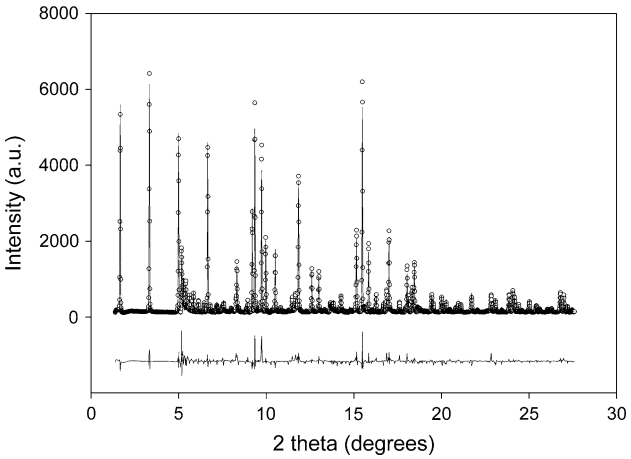

Fig. 6 Rietveld refinement of Cr-chlorite, using the structural model of Brown and Bailey (1963). Synchrotron X-ray diffraction, $\lambda = 0.4142$ Å

$(Mg_4Al_4Si_2O_{10}(OH)_8)$, decreases with pressure and increases with temperature. This observation is in agreement with the experimental results obtained by Pawley (2003, her Fig. 2), as predicted by the model of Baker and Holland (1996) along the univariant reaction (4). In Fig. 7b, the effect of the $CrAl_{-1}$ exchange is plotted and compared with available experimental data in complex peridotite systems and with natural occurrences (Brown and Bailey 1963; Phillips et al. 1980; and references therein). The diagram shows that chlorite in equilibrium with a mantle assemblage has a limited content of Cr_2O_3, that is below 2 wt%.

Orthopyroxene

Orthopyroxenes, normalized on the basis of 6 oxygens, are $Mg_2Si_2O_6$ enstatites with a small component of Al and Cr (see Supplementary data). Orthopyroxene accepts Al through the substitution of the Tschermak component ($MgAl_2SiO_6$); Cr is incorporated via $CrAl_{-1}$ in the octahedral sites, according to crystal field theory and simple crystal-chemical considerations (Klemme and O'Neill 2000; Canil and O'Neill 1996, Burns 1993). The results of this experimental study have been plotted in the diagram Al versus Cr (Fig. 8) and are compared with previous experimental results (Klemme and O'Neill 2000; Brey et al. 1999). Present data are consistent in terms of Al/Cr ratio and comparable as a function of bulk X_{Cr} with previous results.

Spinel and pyrope

Spinels are solid solutions between magnesiochromite ($MgCr_2O_4$) and spinel s.s. ($MgAl_2O_4$), X_{Cr} (Cr/(Cr + Al)) describing their mineral chemistry. Overall, Cr decreases with increasing pressure and temperature. However, different bulk compositions and, above all, different coexisting phases strongly affect the composition of spinels (see Supplementary data). In bulk compositions B and C, where spinel coexists with enstatite, X_{Cr} reveals a strong Cr fractionation into spinel, only limited variations as a function of P and T are observed; in bulk A, where spinel coexists with garnet, large variations occur as a function of P and T.

Pyrope contains very low knorringite component, with Cr/(Cr + Al) from 0.05 to 0.03 even at the highest temperature investigated (see Supplementary data). Knorringite component in garnets is markedly lower than in both experimental studies at higher temperatures and natural occurrences in ultramafic xenoliths or natural diamonds form kimberlites (Nixon and Hornung 1968; Stachel and Harris 2008).

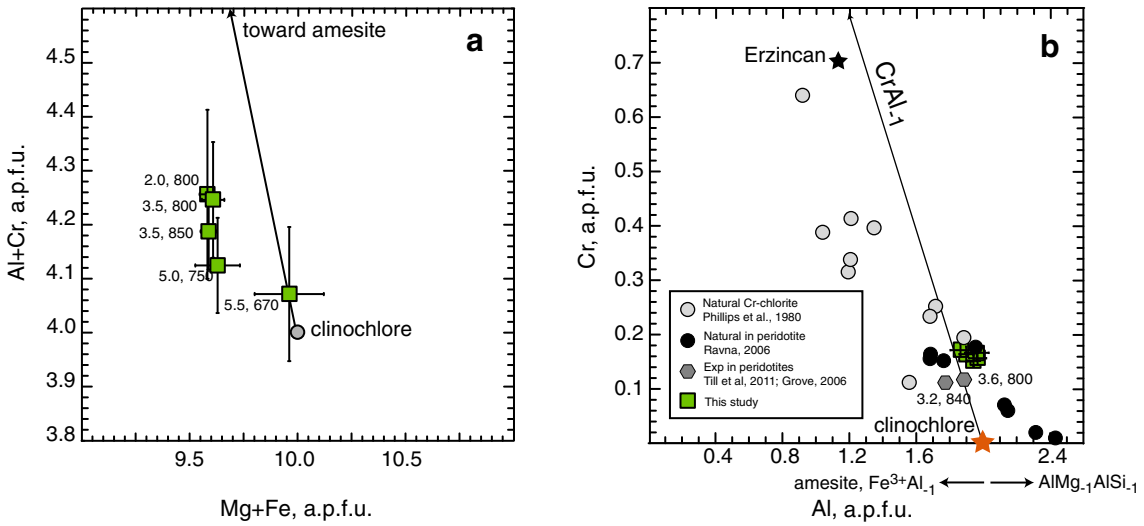

Fig. 7 Mineral chemistry of chlorite: **a** (Mg + Fe) versus (Al + Cr) in a.p.f.u. The *arrow* from clinochlore toward amesite component represents the Tschermak exchange vector; **b** Cr versus Al diagram of experimental results of this study as compared to natural occurrences and previous experimental results in complex peridotite systems. Natural occurrences include chlorite found in mantle rocks, i.e., dunites, in intergrowths of olivine and chromite, e.g., Day Book Body, North Carolina), and from hydrothermal environments, i.e., vugs, veins, and other openings in serpentine associated with chromite ore (e.g., Erzincan, Turkey; Niggihalli Belt shists, India)

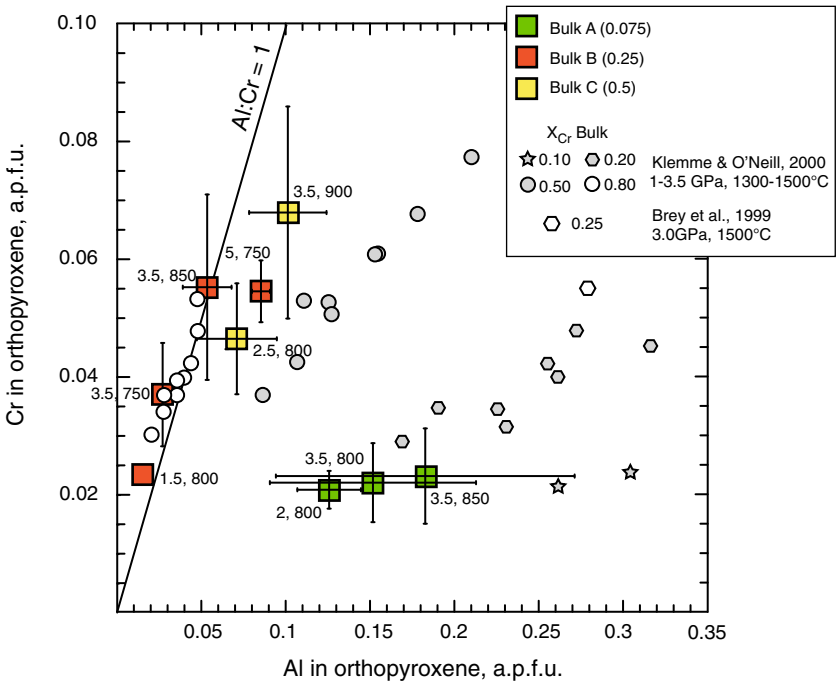

Fig. 8 Mineral chemistry of orthopyroxene. Al versus Cr in a.p.f.u. compared with previous experimental studies

Mg-sursassite, phase-HAPY, and 11.5 Å phase

Chemical analyses of Mg-sursassite are normalized to 16 cations and 28 oxygens, according to the formula $Mg_5Al_5Si_6O_{21}(OH)_7$. Following Gottschalk et al. (2000), who re-named MgMgAl-pumpellyite first synthesized by Schreyer et al. (1986) and further investigated by Fockenberg (1998) and Artioli et al. (1999), Mg-sursassite is characterized by the isostructural phase Mn-sursassite ($Mn_4Al_2Al_4Si_6O_{22}(OH)_6$), in which not only Mg substitutes for Mn but also Al is replaced by Mg + H. Previous results, however, also suggest a continuously variable composition with Mg:Al:Si ratios ranging from 5.28:5.02:5.81 (Bromiley and Pawley 2002) to 4.87:5.17:5.93 (Fockenberg 1998). The addition of Cr might imply the additional substitution Al = Cr assuming

all Cr to occur as Cr^{3+}. As a result, Mg-sursassite is expected to have a complex solid solution. Chemical analysis of the Mg-sursassite of the present study ($Mg_{5.5}Al_{4.4}Cr_{0.2}Si_{5.8}$ $O_{21}(OH)_7$) reveals a ratio Mg:(Al + Cr):Si = 5.55:4.61:5.82, enriched in Mg and depleted in Al + Cr. Cr has previously never been reported in the crystal structure of Mg-sursassite. Present results suggest that at 6 GPa, 650 °C Mg-sursassite can host up to 1.9 wt% of Cr_2O_3 (0.22 Cr a.p.f.u.). However, chemical data have large uncertainties due to the analytical difficulties in fine-grained samples, and further experiments are required to better characterize the crystal chemistry of Mg-sursassite in the presence of chromium.

Phase-HAPY ($Mg_{2.1}Al_{0.9}(OH)_2$ $Al_{0.9}Si_{1.1}O_6$) has been very recently investigated and its structure defined on the basis of run products obtained in the system MASH. Gemmi et al. (2011) determined its structure by the automated electron diffraction tomography method and refined its structure by synchrotron X-ray powder diffraction. Phase-HAPY is a single-chain hydrous silicate, with a topology closely related to pyroxenes. The difference consists in the presence of an additional cation site in the octahedral layer, which expands the structure perpendicular to the alignment of the tetrahedral chains and, consequently, a negative charge balanced by the presence of hydrogen in OH groups (Gemmi et al. 2011). Likely substitutions expected in phase-HAPY further indicate that this phase might be of relevance in a variety of ultramafic bulk compositions. In the Cr-bearing system, phase-HAPY has been identified by X-ray powder diffraction. Microprobe analysis shows that phase-HAPY can host from 3.21 (5.2 GPa, 700 °C) to 2.67 (5.4 GPa, 720 °C) wt% of Cr_2O_3, values that translate, after a normalization based on 5 cations and 7 oxygens, to 0.11–0.09 a.p.f.u. (see Supplementary data). As compared to the previously defined hydrate (Gemmi et al. 2011) found in the MASH system, Cr-bearing phase-HAPY—$Mg_{2.2}Al_{1.5}Cr_{0.1}Si_{1.1}O_6(OH)_2$—is enriched in Mg, with 2.2 compared with 2.1 a.p.f.u., while Al is lower, with 1.5 compared to 1.8 a.p.f.u..

The chemical analysis of the 11.5 Å phase suggests a quite homogeneous mineral chemistry both in the Cr–MASH and in the MASH system. Cr_2O_3 ranges from 1.76 to 1.87 wt% at 6 GPa, 650 °C and 6.5 GPa, 700 °C, respectively. Totals suggest a particularly large amount of water, estimated to be 14–15wt%. Microprobe analysis suggests a very reproducible mineral chemistry with MgO = 46.5 wt%, Al_2O_3 = 10.8 wt%, SiO_2 = 26.3 wt%, and Cr_2O_3 = 1.76 wt%, at 6.0 GPa, 650 °C; and MgO = 46.3 wt%, Al_2O_3 = 11.0 wt%, SiO_2 = 26.8 wt%, and Cr_2O_3 = 1.87 wt%, at 6.5 GPa, 700 °C, corresponding approximately to a composition with Mg/Al/Si ratios of 6.3:1.2:2.4.

Discussion

The effect of Cr on phase equilibria as compared to the simple MASH system

The addition of Cr into the simple MASH system adds new constraints on phase equilibria relevant for modeling transformations in a hydrated lithospheric mantle and in Al-rich compositions of subduction mélanges. No additional Cr-bearing phases were found within the stability field of chlorite, indicating that phase equilibria are mostly affected by continuous reactions. Univariant reactions in the system MASH change to divariant fields in the more complex Cr-bearing system. All phases can host Cr into their structure although to different extents. The *P–T* location and the width of divariant fields are strongly related to the Cr partitioning among all phases. Present results suggest that for bulk A (X_{Cr} = 0.075), Cr–Al partitioning follows the order: spinel > orthopyroxene > chlorite ≥ phase-HAPY > garnet. In particular, at 5 GPa, 750 °C (bulk with X_{Cr} = 0.075) equilibrium values are $X_{Cr}^{spinel} = 0.27$, $X_{Cr}^{chlorite} = 0.08$, $X_{Cr}^{garnet} = 0.05$; at 5.4 GPa, 720 °C the values are $X_{Cr}^{spinel} = 0.33$, $X_{Cr}^{HAPY} = 0.06$, and $X_{Cr}^{garnet} = 0.04$; and at 3.5 GPa, 850 °C $X_{Cr}^{opx} = 0.12$ and $X_{Cr}^{chlorite} = 0.07$.

Cr solubility in chlorite is limited to less than 2 wt%, and its effect is to shift reaction (4) to slightly higher temperature, e.g., between 850 and 900 °C, at 3.5 GPa, as compared to 830 °C as suggested by Pawley (2003) for the system MASH (Fig. 3). Therefore, the divariant field representing the transformation of chlorite + enstatite to the anhydrous assemblage garnet, spinel, and forsterite is limited in temperature. The presence of Cr strongly favors the stability of spinel, which is an almost ubiquitous phase. Spinel coexists with garnet, forsterite, and chlorite up to 5.5 GPa, 670 °C and 5 GPa, 700 °C, suggesting that chlorite persists to slightly higher pressure compared with the simple system MASH (see Fig. 1).

Experimental results obtained here were used to complete a chemographic analysis projecting coexisting phases from H_2O, i.e., fluid-saturated conditions in the system MgO–Al_2O_3–SiO_2–Cr_2O_3 (Fig. 9). From 2 to 3.5 GPa and 800 to 850 °C, the chlorite + orthopyroxene join is stable; therefore, as a function of bulk compositions, the 4-phase assemblages chlorite–orthopyroxene–spinel–forsterite and chlorite–orthopyroxene–spinel–garnet are possible. At 5.5 GPa and 670 °C, we observe the assemblage chlorite–garnet–spinel–forsterite (blue tetrahedron in Fig. 9) which implies an overstepping of the reaction

$$\text{chlorite} + \text{orthopyroxene} = \text{garnet} + \text{spinel} + \text{forsterite} + H_2O,$$

the latter assemblage is represented by the light-blue plane in Fig. 9.

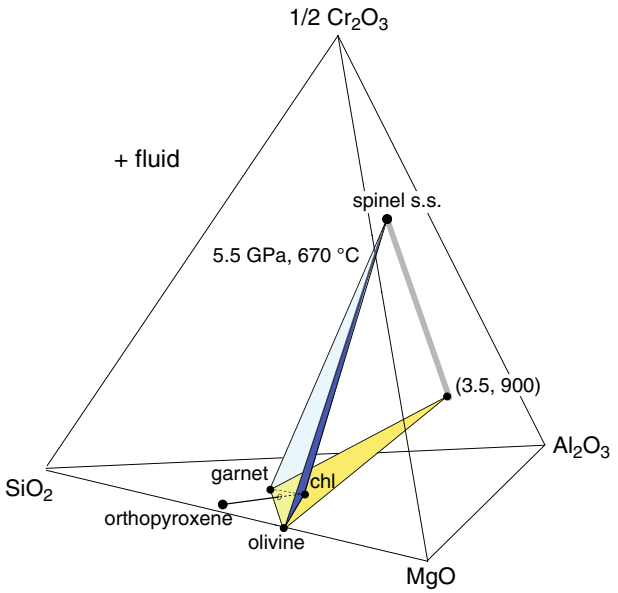

Fig. 9 Chemographic analysis of coexisting phases in the system Cr–MASH at fluid-saturated conditions. See text for further details

Despite the addition of Cr_2O_3 to the model system MASH, the terminal reaction that indicates the ultimate breakdown of chlorite appears still related to the reaction (3),

$$\text{chlorite} = \text{forsterite} + \text{garnet} + \text{spinel} + H_2O,$$

as a result of compositional degeneracy between garnet, olivine, chlorite, and spinel as shown by the yellow plane in Fig. 9. The stoichiometry of this reaction is consequently affected by chemical variations of the phases involved with P and T.

The stability of Cr-bearing chlorite is not fully constrained and based only on synthesis experiments. Nonetheless, our results show that the stability of chlorite is driven by the disappearance of the chlorite + orthopyroxene assemblage (of relevance for mantle rock compositions). The stability of chlorite on its own bulk composition is driven by the terminal reaction that is very close in *P–T* space. A more rigorous prediction of the pressure temperature stability of the 4-phase assemblage chlorite–garnet–spinel–forsterite prior to the terminal reaction of the hydrous phase would be strongly dependent on the Cr–Al partitioning of all phases involved and on solid solution models, still needing to be comprehensively investigated, especially for chlorite solid solutions.

The role of the newly synthesized phase-HAPY: implications for high-pressure phase equilibria in MASH and Cr–MASH systems

Phase relationships in the high-pressure region of the *P–T* space investigated here are strongly affected by the occurrence of the newly synthesized phase-HAPY. Figure 10 shows a possible topology of the reactions in the model system MASH, with emphasis on the location of invariant points involving phase-HAPY. Schreinemakers' analysis is consistent also with experimental results in the Cr-bearing system: colored phase fields in Fig. 10 represent the stable assemblage in the Cr–MASH system.

With respect to phase equilibria usually taken as a reference frame in the MASH system (Fig. 1), invariant point IV is slightly modified here to take into account more recent experimental constraints of Bromiley and Pawley (2002). Invariant points II and III should be reconsidered in the light of the addition of phase-HAPY. Three new invariant points A, B, and C are required to reconcile the new experimental results presented here. They are expected to be stable within a restricted range of pressure and temperature, approaching invariant point I. The invariant point A (chlorite, forsterite, pyrope, spinel, and phase-HAPY) is generated by the intersection of chlorite terminal reaction (3) with the stability field of phase-HAPY. The invariant point B describes the relations involving Mg-sursassite, as generated by the reaction forsterite + Mg-sursassite = chlorite + pyrope (B3), departing from invariant point IV, and, again, the stability field of phase-HAPY. Invariant point C, only partially constrained experimentally, is required in order to predict the assemblage forsterite + diaspore observed in the present study at 6.5 GPa, 700 °C although this implies that reaction (5) (see Fig. 1), marking the stability of forsterite + diaspore/corundum assemblages, should be shifted toward lower temperature with respect to previous reports by Fockenberg (1995). The Schreinemakers' analysis combined with the present data suggests that beyond the stability of chlorite, a restricted field of stability of phase-HAPY is found. The appearance of phase-HAPY above the stability of chlorite (Gemmi et al. 2011) is controlled, in the MASH system, by the reaction

$$13\,\text{chlorite} = 16\,\text{forsterite} + 4\,\text{pyrope} + 10\,\text{phase-HAPY} + 55\,H_2O\ (\text{A2}).$$

The thermal stability of phase-HAPY is governed, within the stability field of forsterite + diaspore join, by the reaction

$$30\,\text{phase HAPY} = 30\,\text{forsterite} + 1\,\text{pyrope} + 52\,\text{diaspore} + 4H_2O\ (\text{C1}),$$

and at higher temperatures, by the reaction

$$20\,\text{phase-HAPY} = 7\,\text{forsterite} + 5\,\text{pyrope} + 13\,\text{spinel} + 20\,H_2O\ (\text{A1}).$$

Cr–Al partitioning and the spinel- to garnet-peridotite transition: low-temperature constraints

Our results provide additional information on the spinel- to garnet-peridotite transition in the mantle, adding important

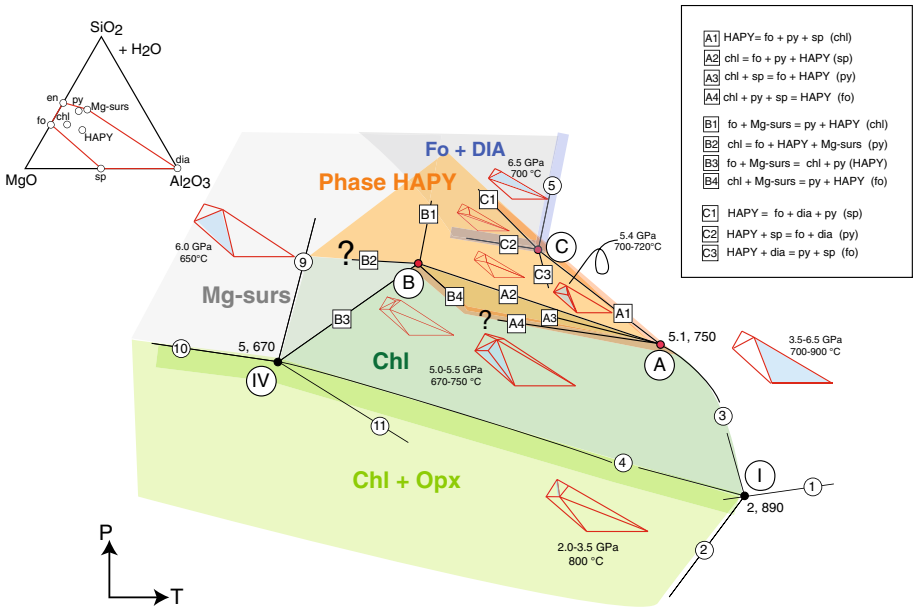

Fig. 10 Schreinemakers' analysis showing the possible topology of phase relations in the MASH system involving phase-HAPY. Colored phase fields in chemographies represent experimental assemblages found in the Cr–MASH system at the indicated *P–T* conditions with which the topology is consistent

constraints at low temperatures. Indeed, although the effect of Cr on the spinel- to garnet-peridotite transition has been extensively investigated both experimentally and theoretically by thermodynamic calculations (see Klemme 2004 and references therein, Ziberna et al. 2013), its pressure at relatively low temperatures is still poorly constrained. Klemme (2004) investigated the reaction spinel + orthopyroxene = garnet + olivine in the Cr–MASH system from 1,200 to 1,600 °C over a range of pressure between 4.5 and 16 GPa and confirmed conclusions reached by Webb and Wood (1986): in fertile compositions, i.e., in bulk compositions with $0 < X_{Cr} < 0.2$, the divariant field where spinel and garnet coexist is narrow. In more depleted bulk compositions, i.e., for $X_{Cr} > 0.2$, the effect of Cr becomes of greater importance. Cr–Al partitioning data between spinel and garnet are shown in Fig. 11 and compared with the loop for 1,100 °C reported by Webb and Wood (1986) and Klemme (2004). At low temperatures, the spinel- to garnet-peridotite divariant field is largely displaced to higher pressure, because of the relatively low chromium content present in both spinel and garnet. As a result, we expect that the spinel phase boundary should have a markedly negative *P–T* slope. Although Klemme (2004) defined experimentally a negative slope in the Al-free system $MgO–Cr_2O_3–SiO_2$ (MCR), consistent with results derived by thermodynamic extrapolations by Doroshev et al. (1997) and Girnis and Brey (1999), a positive slope is predicted in the MASH system. On the other hand, Niida and Green (1999) in a synthetic model "MORB-lherzolite" with $X_{Cr} = 0.065$ found that the transformation from spinel- to garnet-bearing assemblages occurred at approx. 2 GPa between 925 and 1,050 °C with a slightly negative slope for this transition. A negative dP/dT slope for the spinel- to garnet-peridotite transition at low temperatures has been envisaged also by Wood and Yuen (1983) and further discussed by Webb and Wood (1986) to account for the observed uplift of old oceanic lithosphere as a result of a lowering of density due to garnet transforming into spinel on cooling at temperature of less than 900 °C (i.e., on aging of the lithosphere). Furthermore, in agreement with experimental results of this study, Ziberna et al. (2013) have recently evaluated the effect of bulk composition on the spinel- to garnet-peridotite

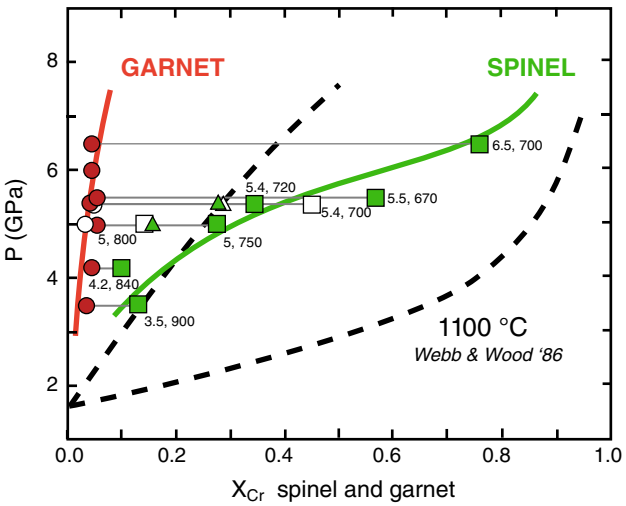

Fig. 11 X_{Cr} versus pressure in experimental spinels and garnets. Present results are compared with high-temperature loop (1,100 °C) reported by Webb and Wood (1986). *Triangles* refer to X_{Cr} as derived by X-ray diffraction refinements of lattice parameter a and applying the equation: a (Å) = 8.086 + 0.25 X_{Cr} spinel (Webb and Wood 1986)

transition and suggested that the depth and the width of the transition in a multi-component system are strongly related to the thermal state of the lithosphere. In the present study, the negative *P–T* slope is obvious and was calculated to be 0.5 GPa/100 °C, similar to the value given by Klemme (2004) in the Al-free MgO–Cr_2O_3–SiO_2 system. However, the dependence of the dP/dT slope on knorringite and chromite components in garnet and spinel, and its dependence on temperature, remains to be resolved experimentally.

Phase assemblages in subduction mélanges and H_2O transfer to deep mantle

We use the phase boundaries from spinel peridotite, to spinel–garnet peridotite and to garnet peridotite, as modeled by Ziberna et al. 2013 for two bulk compositions (gray shaded field in Fig. 12, bounded by $X_{Cr} = 0.04$ and $X_{Cr} = 0.32$), and combine these data with hydrous phase stabilities as determined in this study (Fig. 12) to infer phase assemblages and H_2O transfer in a subduction zone mélange. Phase equilibria are compared with a schematic subarc *P–T* profile (dashed–dotted line in Fig. 12) retrieved from numerical modelling of subduction zones (Gerya and Meilick 2011) and with *P–T* paths for slab surfaces (orange area), at variable mechanical decoupling settings as modeled by Arcay et al. (2007).

Although the mantle wedge is entirely in the garnet stability field, spinel is expected to be the major Cr-bearing phase within the subduction mélange at the slab–mantle interface, both in the chlorite and in phase-HAPY stability fields. Spinel in subduction mélanges should, therefore, not be necessarily regarded as a retrogression product of high-pressure assemblages, but we expect spinel to be a prograde phase coexisting with hydrous phases at subarc depth.

Weighted mass balance calculations were performed in order to constrain the water budget stored in phase-HAPY-bearing assemblages. Note that the H_2O component and the fluid phase have not been used in the calculations, and Monte Carlo simulations have been employed for error propagation (Fumagalli et al. 2009). At 5.4 GPa, 720 °C, bulk composition A gives the following phase abundances: phase-HAPY = 37.2 wt% (±5.5), garnet = 28.3 wt% (±5.8), olivine = 32.2 wt% (±2.1), and spinel = 2.3 wt% (±0.6). Similar results have been obtained at 5.4 GPa, 700 °C. Representative *P–T* paths for a slab–mantle interface show that chlorite schists in subduction mélange move from the chlorite field to a phase-HAPY + olivine + spinel + garnet field, liberating approximately 10.5 wt% H_2O at chlorite breakdown, but still conserving 2.6 (±0.4) wt% H_2O, therefore possibly promoting a link to the

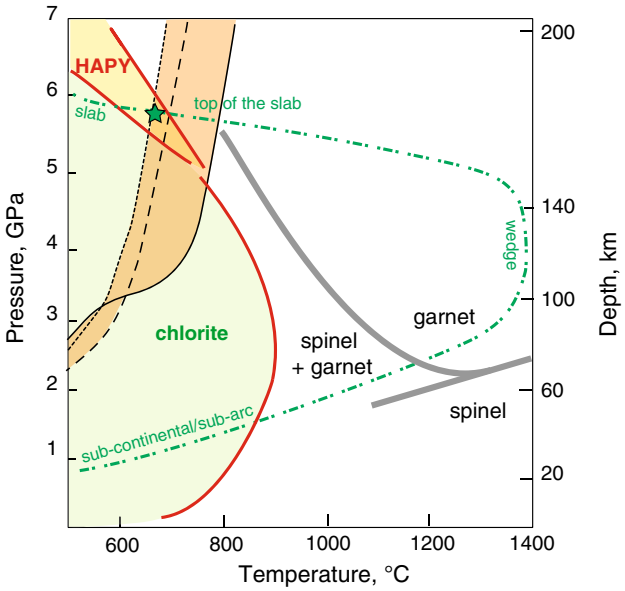

Fig. 12 Schematic phase stability field of chlorite and phase-HAPY are compared with the vertical pressure–temperature profile (*dashed–dotted line*) for a subduction zone beneath the volcanic arc after numerical modeling of Gerya and Meilick (2011) and with *P–T* paths for the slab surface (*orange area*) from Arcay et al. (2007); different paths take into account different water-weakening effect on mantle rocks; *solid line* represents a model reference for a "dry" rock; *dashed line* refers to a moderate rock strength reduction due to water, while *narrow dashed line* to a relevant strength reduction. The stability field of chlorite at low pressure is taken from Ulmer and Trommsdorff (1999). Schematic fields for spinel-peridotite, spinel + garnet-peridotite and garnet-peridotite are inferred from thermodynamic modeling of Ziberna et al. 2013 consistent with the results of this study (*gray lines*)

so-called alphabet phases, notably phase A, above 6 GPa (Ulmer and Trommsdorff 1999).

Conclusions

Experimental results in the simple Cr–MASH system of the present study reveal that the Cr solubility in chlorite in equilibrium with a mantle assemblage is limited to 2.2 wt% Cr_2O_3. Nonetheless, as a result of addition of Cr, the stability field of chlorite is enhanced by approximately 50 °C per 0.5 GPa as compared to the MASH system. Cr–Al partitioning between spinel and garnet suggests a negative d*P*/d*T* slope (approx. 0.5 GPa/100 °C) for the spinel- to garnet-peridotite transition at $T = 670$–900 °C. At high pressures, and $T \leq 750$ °C the breakdown reactions of chlorite involve the formation of phase-HAPY, a hydrous Al-bearing pyroxene-like structure (Gemmi et al. 2011) synthesized here for the first time in the Cr–MASH system. We find a new hydrous phase that coexists with pyrope and spinel at pressures exceeding the chlorite stability. This

may be important for the storage of H_2O in the mantle and for transport of H_2O in subduction zones.

Acknowledgments The authors wish to thank Andrea Risplendente for assistance at electron microprobe. The authors are thankful to H. Marschall, S. Klemme, and D. Jenkins for their review and to Max W. Schmidt for his valuable work as editor. The authors acknowledge ESRF for experimental activity (EC734 experiment; BM08 and ID09 in-house research time). This work was supported by the Italian Ministry of Education, University and Research (MIUR) [PRIN-2009XRH8JJ].

References

Arcay D, Tric E, Doin M-P (2007) Slab surface temperature in subduction zones: influence of the interplate decoupling depth and upper plate thinning processes. Earth Planet Sci Lett 255:324–338

Artioli G, Fumagalli P, Poli S (1999) The crystal structure of $Mg8(Mg_2Al_2)Al_8Si_{12}(O, OH)56$ pumpellyite and its relevance in ultramafic systems at high pressures. Am Mineral 84:1906–1914

Baker J, Holland TJB (1996) Experimental reversals in chlorite compositions in divariant $MgO+Al_2O_3+SiO_2+H_2O$ assemblages. Am Mineral 81:676–684

Bebout GE (2007) Metamorphic chemical geodynamics of subduction zones. Earth Planet Sci Lett 260:373–393

Brey GP, Doroshev AM, Girnis AV, Turkin AI (1999) Garnet–spinel–olivine–orthopyroxene equilibria in the $FeO–MgO–Al_2O_3–SiO_2–Cr_2O_3$ system: I. Composition and molar volumes of minerals. Eur J Mineral 11:599–617

Bromiley GD, Pawley AR (2002) The high-pressure stability of Mg-sursassite in a model hydrous peridotite: a possible mechanism for the deep subduction of significant volumes of H_2O. Contrib Mineral Petrol 142:714–723

Brown BE, Bailey SW (1963) Chlorite polytypism: II. Crystal structure of a one-layer Cr-chlorite. Am Mineral 48:42–61

Burns RG (1993) Mineralogical applications of crystal field theory, 2nd edn. Cambridge University Press, Cambridge, UK

Canil D, O'Neill HStC (1996) Distribution of ferric iron in some upper-mantle assemblages. J Petrol 37:609–635

Chatterjee ND, Terhart L (1985) Thermodynamic calculation of peridotite phase relations in the system $MgO-Al_2O_3-SiO_2-Cr_2O_3$, with some geological applications. Contrib Mineral Petrol 89:273–284

Doroshev AM, Brey GP, Girnis AV, Turkin AI, Kogarko LN (1997) Pyrope-knorringite garnets in the Earth's Mantle: experiments in the $MgO–Al_2O_3–SiO_2–Cr_2O_3$ system. Russ Geol Geophys 38:559–586

Fockenberg T (1995) New experimental results up to 100 kbar in the system $MgO–Al_2O_3–SiO_2–H_2O$ (MASH): preliminary stability fields of chlorite, chloritoid, staurolite, MgMgAl-pumpellyite, and pyrope. Bochumer Geologische und Geotechnische Arbeiten 44:39–44

Fockenberg T (1998) An experimental study of the pressure-temperature stability of MgMgAl-pumpellyite in the system $MgO–Al_2O_3–SiO_2–H_2O$. Am Mineral 83:220–227

Fockenberg T (2008) Pressure-temperature stability of pyrope in the system $MgO–Al_2O_3–SiO_2–H_2O$. Eur J Mineral 20:735–744

Fumagalli P, Poli S (1999) Phase relationships in hydrous peridotites at high pressure: preliminary results of multianvil experiments. Per Mineral 68:275–286

Fumagalli P, Poli S (2005) Experimentally determined phase relations in hydrous peridotites to 6.5 GPa and their consequences on the dynamics of subduction zones. J Petrol 45:1–24

Fumagalli P, Zanchetta S, Poli S (2009) Alkali in phlogopite and amphibole and their effects on phase relations in metasomatized peridotites: a high-pressure study. Contrib Mineral Petrol 158:723–737

Gemmi M, Fischer JK, Merlini M, Poli S, Fumagalli P, Mugnaioli E, Kolbe U (2011) A new hydrous Al-bearing pyroxene as a water carrier in subduction zones. Earth Planet Sci Lett 310:422–428

Gerya TV, Meilick FI (2011) Geodynamic regimes of subduction under an active margin: effects of rheological weakening by fluids and melts. J Metamorph Geol 29:7–31

Girnis AV, Brey GP (1999) Garnet-spinel-olivine-orthopyroxene equilibria in the $FeO–MgO–Al_2O_3–SiO_2–Cr_2O_3$ system: II. Thermodynamic analysis. Eur J Mineral 11:619–636

Gottschalk M, Fockenberg T, Grevel K-D, Wunder B, Wirth R, Schreyer W, Maresch WV (2000) Crystal structure of the high-pressure phase $Mg_4(MgAl)Al_4[Si_6O_{21}/(OH)_7]$: an analogue of sursassite. Eur J Mineral 12:935–945

Grove TL, Chatterjee N, Parman SW, Médard E (2006) The influence of H_2O on mantle wedge melting. Earth Planet Sci Lett 249:74–89

Hamilton DL, Henderson CMB (1968) The preparation of silicate composition by gelling method. Mineral Mag 36:832–838

Hammersley AP, Svensson SO, Hanfland M, Fitch AN, Häusermann D (1996) Two-dimensional detector software: from real detector to idealised image or two-theta scan. High Press Res 14:235–248

Hervig RL, Smith JV (1982) Temperature-dependent distribution of Cr between olivine and pyroxenes in lherzolite xenoliths. Contrib Mineral Petrol 81:184–189

Jenkins DM (1981) Experimental phase relations of hydrous peridotites modelled in the system $H_2O–CaO–MgO–Al_2O_3–SiO_2$. Contrib Mineral Petrol 77:166–176

Jenkins DM, Chernosky JV Jr (1986) Phase equilibria and crystallochemical properties of Mg-chlorite. Am Mineral 71:924–936

Klemme S (2004) The influence of Cr on the garnet-spinel transition in the Earth's mantle: experiments in the system $MgO–Cr_2O_3–SiO_2$ and thermodynamic modelling. Lithos 77:639–646

Klemme S, O'Neill HSC (2000) The effect of Cr on the solubility of Al in orthopyroxene: experiments and thermodynamic modelling. Contrib Mineral Petrol 140:84–98

Kumar N, Reisberg L, Zindler A (1996) A major and trace element and Sr, Nd and Os isotopic study of a thick pyroxenite layer from the Beni Bousera ultramafic complex of N. Morocco. Geochim et Cosmochim Acta 60:1429–1444

Lapham DM (1958) Structural and chemical variation in chromium chlorite. Am Mineral 43:921–956

Larson AC, Von Dreele RB (1994) General structure analysis system (GSAS), Los Alamos National Laboratory Report LAUR 86-748

Marschall HR, Schumacher JC (2012) Arc magmas sourced from mélange diapirs in subduction zones. Nat Geosci 15:862–867

Meyer HOA (1975) Chromium and the genesis of diamond. Geochim Cosmochim Acta 39:929–936

Mukasa SB, Shervais JW (1999) Growth of subcontinental lithosphere: evidence from repeated dike injections in the Balmuccia lherzolite massif, Italian Alps. Lithos 48:287–316

Niida K, Green DH (1999) Stability and chemical composition of pargasitic amphibole in MORB pyrolite under upper mantle conditions. Contrib Mineral Petrol 135:18–40

Nixon PH, Hornung G (1968) A new chromium garnet end member, knorringite from kimberlite. Am Mineral 53:1833–1840

O'Neill HStC, Palme H (1998) Composition of the silicatae Earth: implications for accretion and core formation. In: Jackson I (ed) The Earth's mantle: composition, structure and evolution. Cambridge University Press, Cambridge, pp 3–126

Pawley A (2003) Chlorite stability in mantle peridotite: the reaction clinochlore + enstatite = forsterite + pyrope + H_2O. Contrib Mineral Petrol 144:449–456

Peacock SM (2001) Are the lower planes of double seismic zones caused by serpentine dehydration in subducting oceanic mantle? Geology 29:299–302

Pearson DG, Davies GR, Nixon PH (1993) Geochemical constraints on the petrogenesis of diamond facies pyroxenites from Beni Bousera peridotite massif, North Morocco. J Petrol 34:125–172

Phillips TL, Loveless JK, Bailey SW (1980) Cr^{3+} coordination in chlorites; a structural study of ten chromian chlorites. Am Mineral 65:112–122

Ravna EJK (2006) Prograde garnet-bearing ultramafic rocks from the Tromsø Nappe, northern Scandinavian Caledonides. Lithos 92:336–356

Schreyer W, Maresch WV, Medenbach O, Baller T (1986) Calcium-free pumpellyite, a new synthetic hydrous Mg–Al-silicate formed at high pressures. Nature 321:510–511

Sinigoi S, Comin-Chiaramonti P, Demarchi G, Siena F (1983) Differentiation of partial melts in the mantle: evidence from the Balmuccia peridotite, Italy. Contrib Mineral Petrol 82:351–359

Smith D (2010) Antigorite peridotite, metaserpentinite, and other inclusions within diatremes on the Colorado Plateau, SW USA: implications for the mantle wedge during low-angle subduction. J Petrol 51:1355–1379

Sobolev NV, Logvinova AM, Zedgenizov DA, Seryotkin YV, Yefimova ES, Floss C, Taylor LA (2004) Mineral inclusions in microdiamonds and macrodiamonds from kimberlites of Yakutia: a comparative study. Lithos 77:225–242

Spandler C, Hermann J, Faure K, Mavrogenes JA, Arculus RJ (2008) The importance of talc and chlorite ''hybrid'' rocks for volatile recycling through subduction zones; evidence from the high-pressure subduction mélange of New Caledonia. Contrib Mineral Petrol 155:181–198

Stachel T, Harris JW (2008) The origin of cratonic diamonds—constraints from mineral inclusions. Ore Geol Rev 34:5–32

Stalder R, Ulmer P, Thompson AB, Günther D (2001) High pressure fluids in the system $MgO–SiO_2–H_2O$ under upper mantle conditions. Contrib Mineral Petrol 140:607–618

Staudigel H, Schreyer W (1977) The upper thermal stability of clinochlore, $Mg_5Al[AlSi_3O_{10}](OH_8)$, at 10–35 kb PH_2O. Contrib Mineral Petrol 61:187–198

Suzaki J, Akaogi M, Akimoto S, Shimomura O (1985) Garnet-perovskite transformation in $CaGeO_3$: in situ X-ray measurements using synchrotron radiation. Geophys Res Lett 12:729–732

Till C, Grove T, Withers AC (2012) The beginnings of hydrous mantle wedge melting. Contrib Mineral Petrol 163:669–688

Ulmer P, Trommsdorff V (1999) Phase relations of hydrous mantle subducting to 300 km. In: Fei Y-W, Bertka C, Mysen BO (eds) Mantle petrology: field observations and high pressure experimentation: a Tribute to Francis R. (Joe) Boyd. Geochem Soc Spec Publ 6:259–281

Voshage H, Sinigoi S, Mazzucchelli M et al (1988) Isotopic constraints on the origin of ultramafic and mafic dikes in the Balmuccia peridotite (Ivrea Zone). Contrib Mineral Petrol 100:261–267

Webb SA, Wood BJ (1986) Spinel-pyroxene-garnet relationships and their dependence on Cr/Al ratio. Contrib Mineral Petrol 92:471–480

Welch MD, Crichton WA (2005) A high-pressure polytypic transformation in type-I chlorite. Am Mineral 90:1139–1145

Wood BJ, Yuen DA (1983) The role of lithospheric phase transitions on seafloor flattening at old ages. Earth Planet Sci Lett 66:303–314

Zhang J, Li B, Utsumi W, Liebermann RC (1996) *In situ* X-ray observations on the coesite-stishovite transition: reversed phase boundary and kinetics. Phys Chem Minerals 23:1–10

Ziberna L, Klemme S, Nimis P (2013) Garnet and spinel in fertile and depleted mantle: insights from thermodynamic modeling. Contrib Mineral Petrol 166:411–421